TECHNISCHE UNIVERSITÄT
MÜNCHEN

Physik-Department E12 - Dense and strange hadronic matter

Abschlussarbeit im Bachelorstudiengang Physik

Production of antiparticles in p-Pb collisions at $\sqrt{s_{NN}} = 5.02$ TeV measured with ALICE at the LHC

Lucas Córdova Nyffenegger

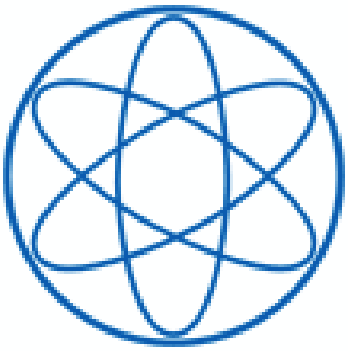

Themensteller:	Prof. Dr. Laura Fabbietti
Betreuer:	M.Sc. Bernhard Hohlweger
Abgabe:	04. Dezember 2017

Abstract

Low-energy antideuterons could be a unique probe for indirect search of dark matter. The interaction of antideuteron with matter, however, needs more investigation. For example there is no scattering data available with any material. One possibility to study it is to analyze the interaction of antideuteron with the detector material of the ALICE detector at the Large Hadron Collider.
In this work the basis is laid by starting out to understand the production of (anti-) protons and (anti-) deuterons in p-Pb collisions at a center of mass energy of $\sqrt{s_{NN}} = 5.02$ TeV. In the course of this analysis, the momentum spectra of protons and their antiparticles showed a kink around 1 GeV/c, which was further investigated and corrected.
Afterwards the efficiency and purity corrected spectra were obtained for protons, deuterons and their corresponding antiparticles.

Zusammenfassung

Niederenergie-Antideuteronen könnten eine einzigartige Probe für die indirekte Suche nach dunkler Materie sein. Die Wechselwirkung von Antideuteron mit Materie benötigt jedoch weitere Untersuchungen. Beispielsweise sind keine Streudaten verfügbar. Eine Möglichkeit dies zu untersuchen, ist die Wechselwirkung von Antideuteron mit dem Detektormaterial des ALICE-Detektors am Large Hadron Collider zu analysieren.
In dieser Arbeit wird die Produktion von (Anti-) Protonen und (Anti-) Deuteronen in p-Pb Kollisionen mit einer Schwerpunktsenergie von $\sqrt{s_{NN}} = 5.02$ TeV untersucht. Im Verlauf der Analyse zeigten die Impulsspektren von Protonen und ihren Antiteilchen einen Knick um 1 GeV/c, der weiter untersucht und anschliessend korrigiert wurde.
Am Ende wurden die mit Effizienz und Reinheit korrigierten Spektren für Protonen, Deuteronen und ihren entsprechenden Antiteilchen erhalten.

Contents

1. Introduction

From observations of the stars such as their luminosity, orbit and the different stages of life they go through, cosmology determines a three-dimensional map of the stars and galaxies and the composition of the various components they are made out of. By observing stars within our galaxy it was seen that the known laws of physics are unable to describe the distribution of velocities of these stars as a function of their distance to the center of the galaxy [1]. So there must probably be some other form of matter to explain the behavior of the stars. This led to the concept of a non interacting bulk of matter, located throughout the universe, so called dark matter. The Millenium Simulation, which is the largest simulation of the growth of dark matter structure ever carried out, uses techniques for following the formation and evolution of the visible components. The results show that dark matter is needed to form the universe of today [2]. Observations indicate that the universe contains 71.4% dark energy, 24% dark matter, and 4.6% "normal" baryonic matter[3]. So only 4% of everything that we see can be described and explained with the known laws of physics. Therefore a lot of research is ongoing in order to understand the nature of dark matter and various kinds of particles were presented as suitable candidates for it. In several experiments, however, no evidence for a particular candidate could be provided so far.

Under the assumption that dark matter particles form standard model particles in the course of their mutual interaction, the indirect search for dark matter looks for the decay and annihilation products into the baryonic channel. Cosmic-ray particles and antiparticles can often be challenging to detect due to a high background signal. Low-energy antideuterons, however, have an ultra-low astrophysical background. In Figure 1.1 the predicted flux of Antideuteron originating from the annihilation of various viable dark matter candidates as a function of the kinetic energy per nucleon can be seen. Additionally, the background contributions to the signal is shown as secondary contributions. The predicted flux exceeds the background flux by more than two orders of magnitude in the energy range below 0.25 GeV/n, and by more than an order of magnitude up to 1 GeV/n. For that reason low-energy antideuterons could be a unique probe for indirect search of dark matter [4].

In this case the preliminary work for the indirect dark matter search is first to understand how antideuteron interacts with matter for example when designing a detector for the dark matter search. When looking at Figure 1.2, one can see that there is no scattering data available in the low-energy range and any scattering data for antideuteron. In

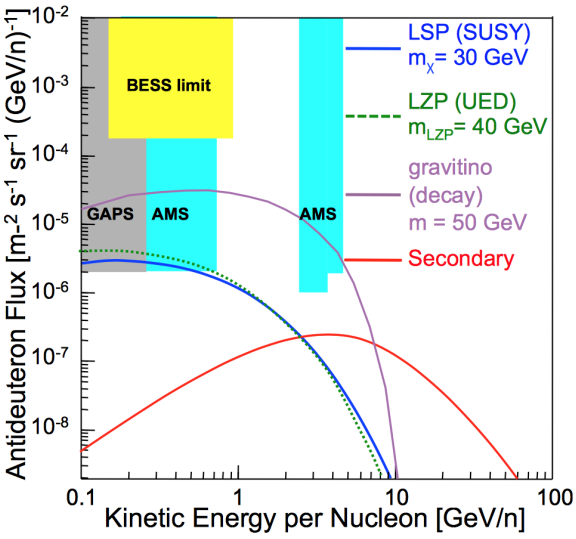

Figure 1.1.: Predicted antideuteron fluxes from different models as a function of the kinetic energy per nucleon. The antideuteron limits from BESS are shown, along with the projected sensitivities of AMS-02 for the superconducting-magnet configuration after 5 years of operation and GAPS after three 35-day flights. The red curve represents the background [4].

collider experiments, such as the LHC, large amounts of antideuterons are produced. The ALICE detector allows to identify and track it from its creation in the collision or form decays. In parts of the setup with high material budget, labeled as TRD in Figure 1.3, its interaction probability can be investigated by analyzing the products with the next detector layer. While the detector system itself will be described in a later section, the basic principal of beforehand described measurement is shown in Figure 1.3.

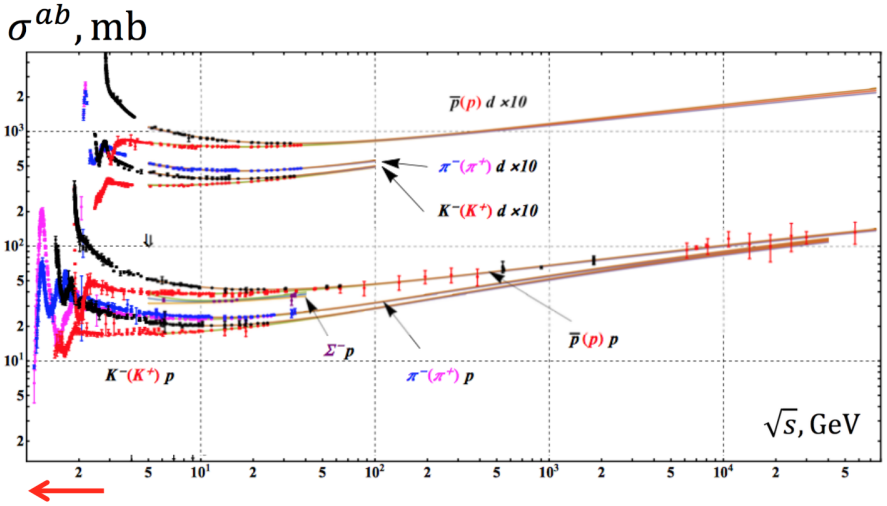

Figure 1.2.: Three upper curves: Cross section of deuteron scattering. The red arrow represents the low energy region [5].

This thesis is structured as follows. The ALICE experiment is presented chapter 2. The analysis is described in chapter 3. In chapter 4 the corresponding results are discussed. The summary and an outlook are given in chapter 5.

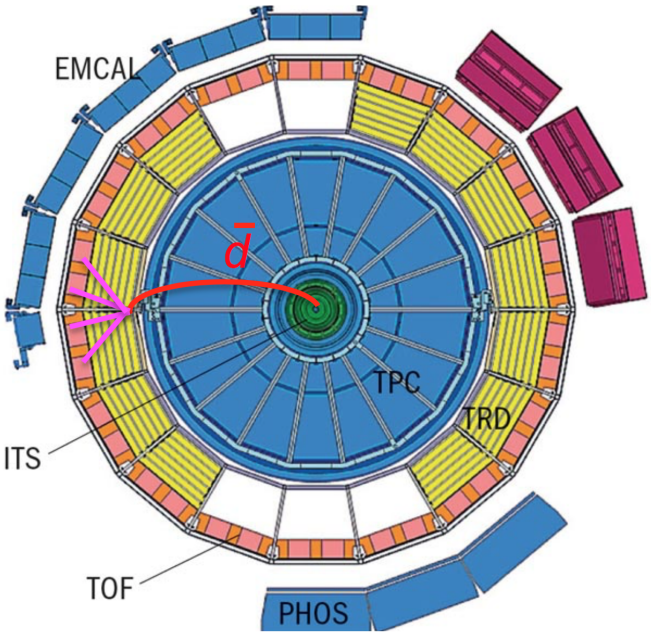

Figure 1.3.: Corss section of ALICE. Idea of a project, where an antideuteron interacts with the TRD material and produces a pion shower, which can be analyzed with the TOF.

2. Experimental Setup

2.1. Large Hadron Collider (LHC)

The LHC was built to create and investigate known and unknown elementary particles as well as new states of matter, starting from the review of the the current standard model of particles.
It has been in operation since 2008 and is located at the European Organization for Nuclear Research (CERN) research center in Geneva, Switzerland. The LHC is set up in a tunnel with a circumference of 27 km and is the last stage of a system of accelerators where either protons are collided at a top center of mass energy of 14 TeV or respectively lead (Pb) ions at a center of mass energy of 5.02 TeV.

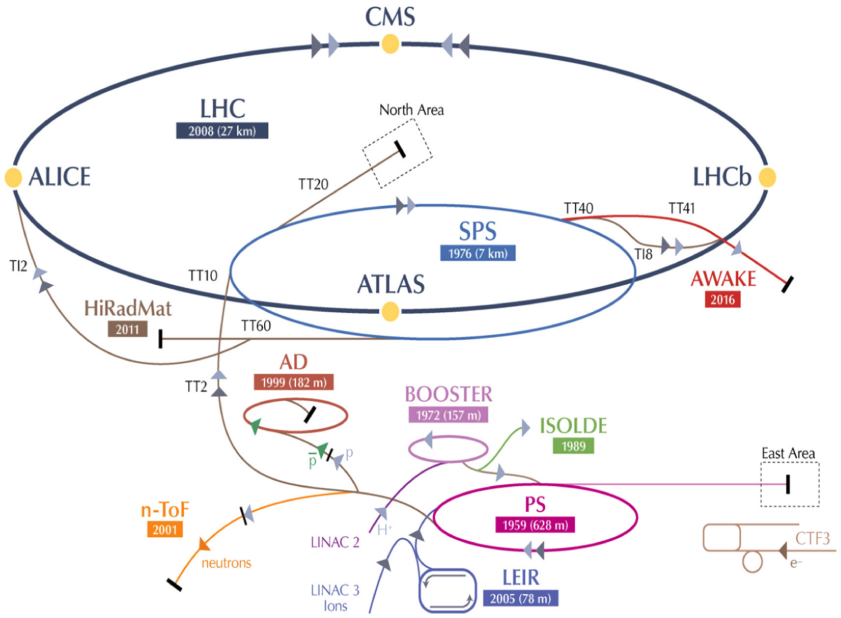

Figure 2.1.: Schematic representation of the accelerator system at CERN [6]

In Figure 2.1 the different pre stages for the acceleration together with the four independent detector systems are shown: A Large Ion Collider Experiment (ALICE), A Toroidal LHC ApparatuS (ATLAS), Large Hadron Collider beauty (LHCb) and Compact Muon Solenoid Experiment (CMS). The work of this thesis is based on the data taken with the ALICE detector, which will be described more closely in the next section.

2.2. A Large Ion Collider Experiment (ALICE)

ALICE is an experiment designed especially for heavy ion collisions, which focuses on the strongly interacting matter at extreme energy densities and the study of Quark Gluon Plasma. In Figure 2.2 the setup of ALICE, with all its subsystems, is shown. The part surrounded by the magnet is called central barrel. This work focusses on the tracking and identification of particles (PID), and therefore the analysis is mainly based on the Time Projection Chamber (TPC) and Time of Flight (TOF).

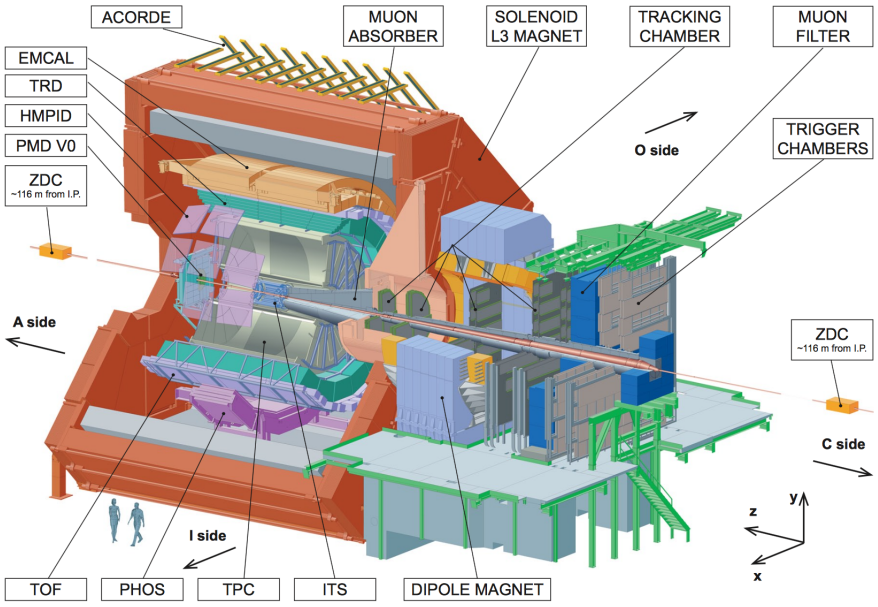

Figure 2.2.: ALICE detector with the labeled subsystems [7]

2.2.1. Time Projection Chamber (TPC)

The ALICE TPC is colored grey in Figure 2.2. Out coming particles from the collision traverse the gas volume in the drift space of the TPC, where charged particles leave an ionization trace in the gas. Due to the voltage applied between the end caps and the central cathode an electric field parallel to the beam pipe separates the electron-ion pairs. The electrons drift towards the readout chambers located at the end caps of the TPC, whereas the ions drift towards the cathode and are neutralized. In order to obtain a measurable signal, the electrons need to be amplified with Multi Wire Proportional Chambers (MWPCs). A high voltage along the wires above the readout pads causes the electrons to create an avalanche, which in turn induce a mirror charge on the segmented readout plane. The signal per readout pad is proportional to the amount of primary electrons and is then passed on to the readout electronics. The number of created electron-ion pairs, produced by the particle traversing the TPC, depends on its energy loss $\langle$ dE / dx $\rangle$ and can be described by the Bethe-Bloch formula:

$$-\left\langle \frac{dE}{dx} \right\rangle = \frac{4\pi n}{m_e c^2 \beta^2} \cdot \left(\frac{ze^2}{4\pi\varepsilon_0} \right)^2 \left[\ln \left(\frac{2m_e c^2 \beta^2}{I \cdot (1-\beta^2)} \right) - \beta^2 \right] \tag{2.1}$$

In this equation $\beta = v/c$ is the fraction of the instantaneous velocity of the particle and speed of light, z the charge of the particle, ε_0 the electric field constant, e the elementary charge , n the electron density, m_e the mass of the electron and I the average excitation potential of the material. By replacing β by the momentum a mass dependence is introduced, and therefore Equation 2.1 can be used for PID. The MWPCs are segmented in 18 separate readout modules in azimuthal direction, with smaller pads at the inner chambers. A maximum of 159 rows in radial direction can provide track points and dE/dx information. Tracks traversing all 159 rows have the best resolution. The detection volume at maximum resolution is $|\eta| \leq 0.9$, while for a pseudorapidity of $0.9 < |\eta| < 1.5$ the number of track points reduces to around a third [8]. In order to measure the momentum of particles originating from the collision, the inner barrel of the TPC is surrounded by a magnetic field with $B \approx 0.5$ T parallel to the beam axis. Due to the Lorentz force the tracks have a curvature and the momentum can be measured. This in turn allows together with the Bethe Bloch formula to identify these particles.

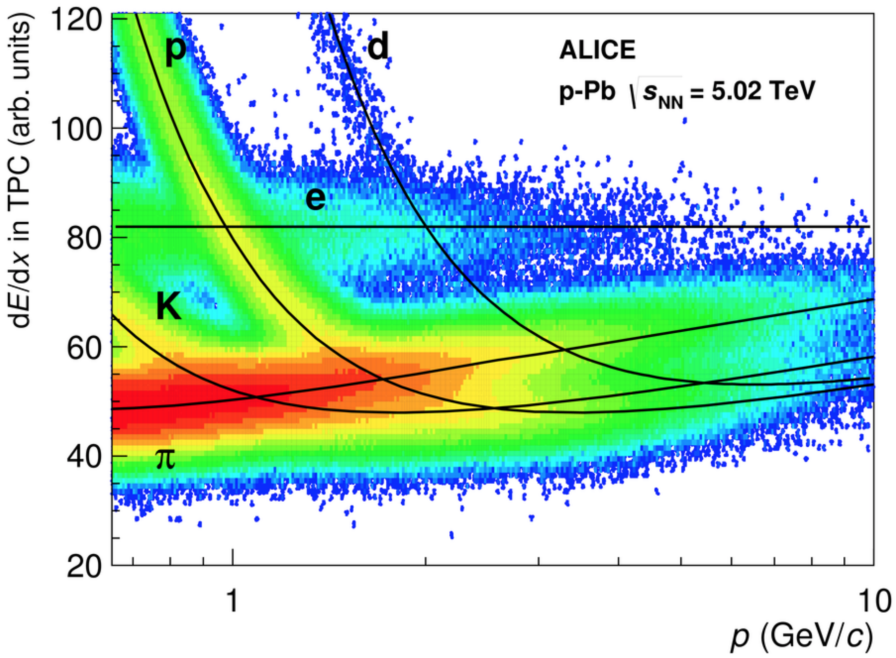

Figure 2.3.: Charged particle specific energy loss (dE/dx) as a function of momentum, as measured in the TPC in p-Pb collisions. The black lines are the corresponding Bethe-Bloch parametrizations for the various particle species. [9]

Figure 2.3 shows the energy loss (dE/dx) distribution as a function of momentum, as measured in the TPC in p-Pb collisions. It can be seen that the detector allows a single particle identification at low momenta. At a momentum of about 1 GeV/c the proton band begins to merge with the pion and kaon band. Deuterons merge at

around 1.7 GeV/c with electrons. From then on, they can only be distinguished with statistical methods. In order to complement the PID in the higher momentum region, the information from another detector, for example the Time of Flight detector, is needed to complement the PID.

2.2.2. Time of Flight (TOF) Detector

The Time of Flight system measures the time a particle takes from the collision to the TOF detector and with the known distance, the velocity can be measured. In Figure 2.2 the TOF is colored in purple. Combined with the momentum measurement of the track, particle identification is possible according to the equation $p = m\beta\gamma$.

It cylindrically covers the collision point at a radius of 3.6 m and is divided into 18 super modules and around 160000 readout pads. With a time resolution of around 100 ps the tracks within the TPC are matched to the TOF signals. The start time for the TOF measurement is provided by the T0 detector, which consists of two arrays of Cherenkov counters T0C and T0A, positioned at opposite sides of the interaction point [10].

The acceptance is in $|\eta| < 0.9$ and 2π in azimuthal direction and particles with a momentum $p > 0.3$ GeV/c can be identified. In Figure 2.4 the β distribution as a function of momentum for particles reaching TOF in p-Pb interactions can be seen. Electrons and pions, which have a low mass, almost reach the speed of light with $\beta = v/c \approx 1$ in the whole momentum range, while heavier particles have lower velocity for low momenta. Tracks with a momentum $p < 0.3$ GeV/c are not able to reach the TOF since they curl up within the TPC volume and do not give a signal. The bands correspond to different particle species and it can be seen that the TOF is able to separate protons from other particles for $p < 2.5$ GeV/c and the deuterons for $p < 5$ GeV/c.

2.2.3. Event reconstruction

For the Event reconstruction the whole ALICE detector system is used. The following paragraph is just a brief overview of the working principal. For a detailed description of the steps the reader is referred to Chapter 6 in [10].
The reconstruction of the vertex and the track, are very important as they allow the PID. In the first step, the clusterization, the detector data are converted into "clusters" characterized by positions, signal amplitudes, signal times, etc., and their associated errors. This process is done separately for each detector. In the next step the preliminary interaction vertex, using tracklets in the first two Inner Tracking System (ITS) layers, is determined. The track reconstruction starts in the next step by applying a Kalman filtering technique [11]. Therefore, tracks are fit to the clusters starting from the outer rim of the TPC inwards, then they are reconstructed again outwards with additional information from e.g. the TOF. Then, in a final fit the reconstructed tracks are refit together in order to determine the final Vertex.

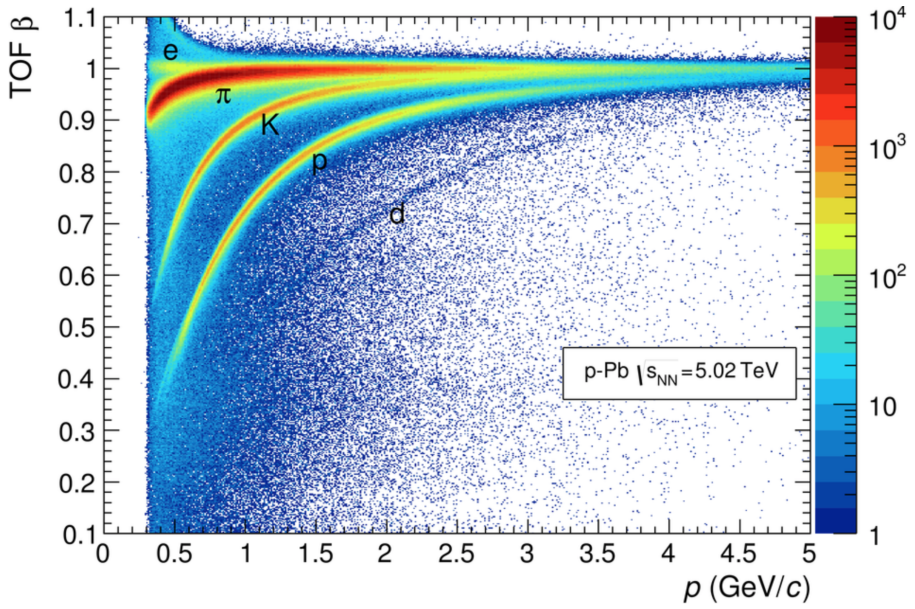

Figure 2.4.: Distribution of β as measured by the TOF detector as a function of momentum for particles reaching TOF in p-Pb interactions [10]

2.2.4. AliRoot

AliRoot is based on the software ROOT developed at CERN. ROOT was written in the computer language C++ and is mainly used in nuclear physics to evaluate experimental data and to display the results graphically. AliRoot extends ROOT with libraries that are specific to ALICE, for example analysis and detector related information. It allows the access to the Analysis Object Data (AOD), which are the processed raw data from the experiment.

3. Analysis Method

3.1. Particle Identification (PID)

Both of the described detectors in section 2.2 allow particle identification. As already mentioned in subsection 2.2.1, the TPC measures the energy loss. The theoretical values of $\left\langle \frac{dE}{dx} \right\rangle$ can be determined by a parameterization of the Bethe Bloch function. Here detector effects have to be taken into account, which are explained in [12]. For the differentiation of the particles species, the numbers of sigma ($n\sigma$) method is used. Here a cut on the relative difference $\Delta \left\langle \frac{dE}{dx} \right\rangle$ of the energy loss value is employed in terms of numbers of standard deviations from the mean.

The energy loss relative to one species from the reconstructed tracks is obtained in transverse momentum (p_T) bins. For one p_T bin this is shown in Figure 3.1 for pions. This in principal is a slice of the spectrum shown in Figure 2.3. For low momenta the contributions of each species are well separated. While for higher momenta, as it is the case in Figure 3.1, the distributions overlap. Subsequently, the distribution is fit with convolution of Gaussian functions for each particle species contribution to the total distribution, where the theoretical values of the energy loss are the mean values for each particle species. This results in a standard deviation σ_{TPC} for each p_T value. All particles that deviate from the mean within the $n\sigma_{TPC}$ range are identified as the searched particle.

For the TOF, the same PID method is used. The theoretical values of the TOF spectrum are determined by the parameterization $p = m_0\beta\gamma$. For $n\sigma_{TOF}$, however, the difference $\Delta\beta$ of the measured velocity and the theoretically determined velocity is now calculated in a p_T interval. After that, it is the same procedure as for $n\sigma_{TPC}$.
The advantage of this method is that the $n\sigma_i$ of both detectors can be combined to a combined TPC and TOF PID, as can be seen in Equation 3.1.

$$n\sigma = \sqrt{(n\sigma_{TPC})^2 + (n\sigma_{TOF})^2} \tag{3.1}$$

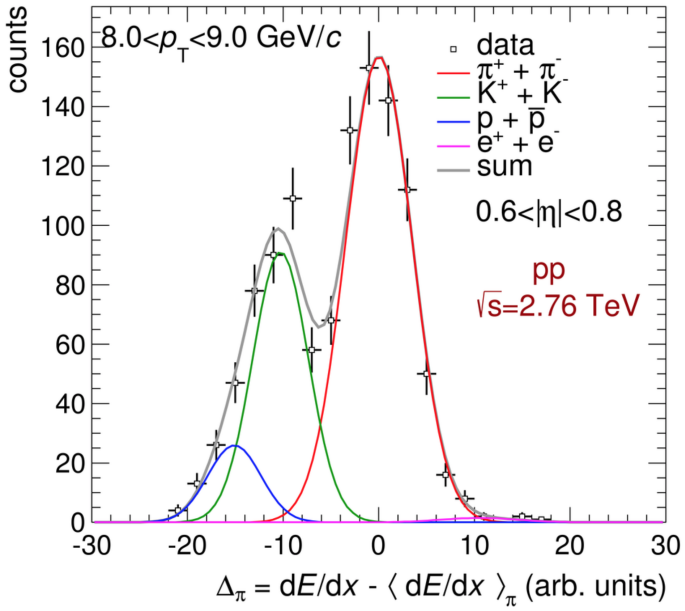

Figure 3.1.: Ionization energy loss (dE/dx) distributions in the TPC in pp collisions at $\sqrt{s_{NN}} = 2.76$ TeV. The lines represent Gaussian fits as described in the text [10].

3.2. Event and track selection

The data used for this analysis were recorded from p-Pb collisions at a center of mass energy of $\sqrt{s_{NN}} = 5.02$ TeV. For good quality data, events and tracks are selected according to certain criteria, so called cuts are implemented. In Table 3.1 the implemented event and track cuts can be seen. As explained in subsection 2.2.3, the vertex of an event is reconstructed by propagating tracks to the collision point, so every event needs to have a vertex and at least two tracks contributing to this vertex. An other requirement is that the vertex must be within 10 cm in z direction from the geometrical center of ALICE.

This work focuses on the identification of (anti-) protons and (anti-) deuterons. Therefore kinematic and topological cuts as well as the PID cuts as discussed according to the $n\sigma$ method were implemented. Tracking within the full acceptance of the central barrel was ensured by selecting tracks within a pseudorapidity range $|\eta| < 0.8$. That way it is ensured that the distribution of tracks in η is more or less flat, as it can be seen in Figure 3.2. To ensure a good energy resolution and a proper fit of the signals by the tracking algorithm a minimum of 100 crossed rows within the TPC is required. The distance of closest approach (DCA) to the primary vertex is required to be smaller than 2.4 cm in x or y and smaller than 3.2 cm along z. For the PID, tracks with $n\sigma < 3$ were identified. At low momenta the TPC is able to identify particles on a track by track basis, only at higher momenta additionally the TOF is required. Up to which momentum the TPC is capable of PID depends on the particle species. For (anti-) protons the TOF was required for momenta $p > 0.7$ GeV/c whereas for (anti-) deuteron a value of $p > 1.4$

GeV/c. In order to be able to require a TOF signal, the track in the TPC has to be matched with this signal, which has a matching efficiency of around 75%. Therefore the number of identified tracks is significantly enhanced when only using the TPC in the momentum region where the main yield sits.

Figure 3.3 shows the momentum distribution after applying all mentioned cuts. The discontinuity at $p = 0.7$ GeV/c and $p = 1.4$ GeV/c are due to the differences in performance when identifying particles with the TPC alone and the combined TPC and TOF information. The kink at $p = 1.0$ GeV/c for (anti-) protons can not be related to that reason, and required further investigation. At first it was investigated if this was reproduced in the simulation and could be corrected by purity and efficiency.

Event cut Parameter		**Value**
Number of contributors to the primary vertex		≥ 2
Vertex in z direction		≤ 10 cm
Track cut Parameter		
Number of TPC clusters per track		≥ 100
DCA_{xy}		≤ 2.4 cm
DCA_z		≤ 3.2 cm
$\lvert\eta\rvert$		≤ 0.8
$n\sigma$		≤ 3
TPC only PID:	for (anti-) proton	$p \leq 0.7$ GeV/c
	for (anti-) deuteron	$p \leq 1.4$ GeV/c
Combined TPC and TOF PID:	for (anti-) proton	$p \geq 0.7$ GeV/c
	for (anti-) deuteron	$p \geq 1.4$ GeV/c

Table 3.1.: Event and Track cut parameters and their respective values.

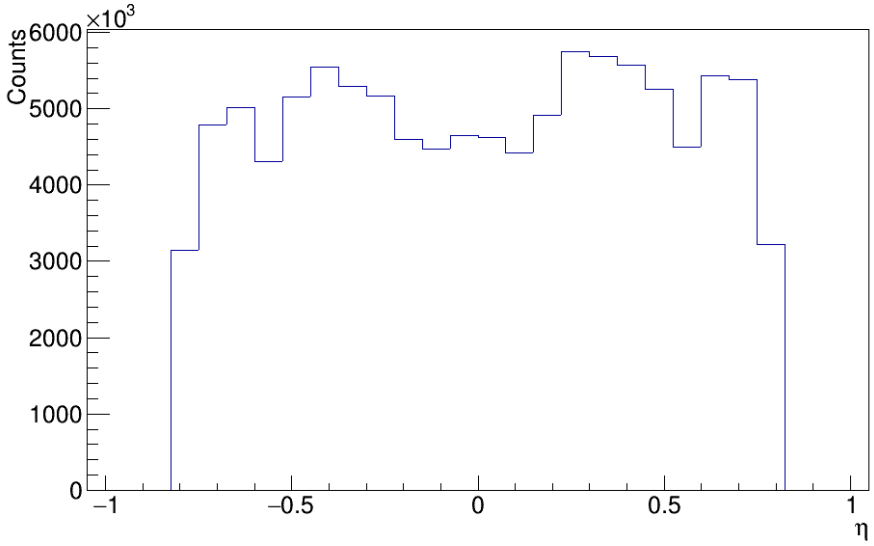

Figure 3.2.: Eta distributions of antiprotons with the cut $|\eta| < 0.8$

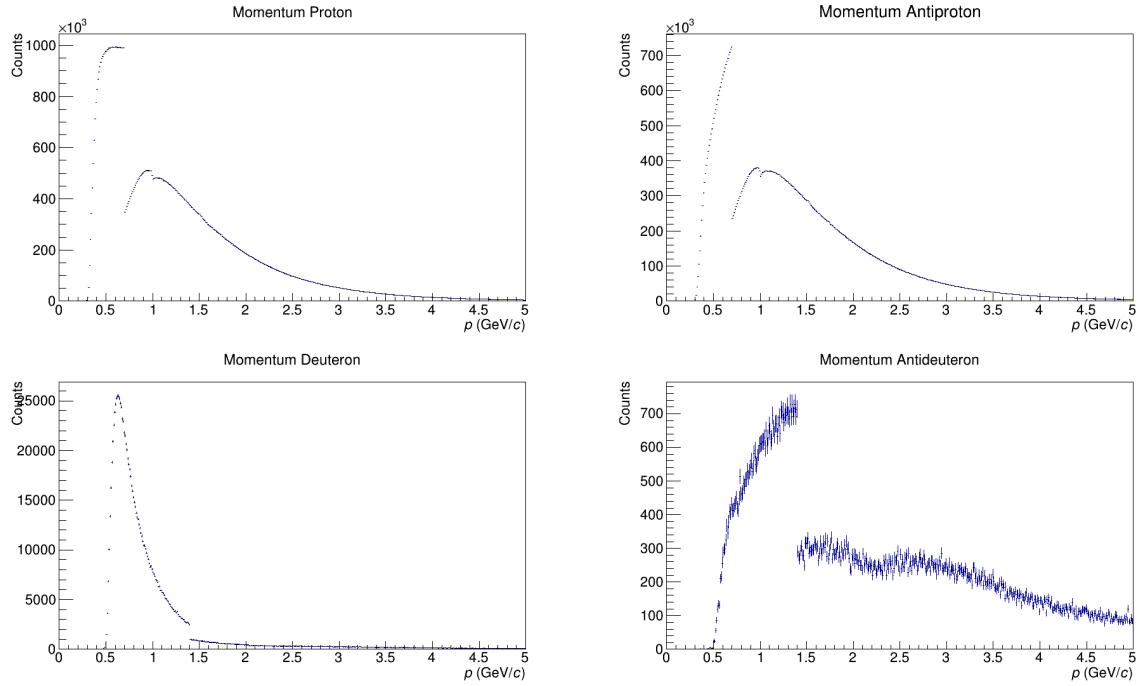

Figure 3.3.: Raw momentum spectra of all particle species after the implemented cuts.

3.3. Monte Carlo Studies

The cuts for this analysis were also used to analyze the Monte Carlo dataset corresponding to the real dataset. In contrast to actual collisions, in the simulation the Monte Carlo truth information can be accessed. For (anti-) protons, the collision is simulated by the DPMJET Monte Carlo event generator [13]. No (anti-) Deuteron is produced in standard simulations and therefore a special production was used where heavy nuclei were added to the EPOS generated events. Both are anchored to the corresponding run period to reproduce the data.
In the following step the response of the various detectors to the particles is simulated by GEANT [14]. These signals are then used to reconstruct the events with the same algorithm employed for real collisions.

The Monte Carlo dataset can be used to understand the effect of the event and track selection. Two quantities are obtained for this purpose, purity and efficiency. The purity quantifies the contribution form other particles to the sample, that could not be excluded by the PID. It is calculated by dividing the amount of correctly identified particles by the amount of selected particles after all cuts. In Figure 3.5 the purity of all particles of interest can be seen. In this Figure the purity depends on p and η and one can see that the purity is flat as a function of η for all particle species. For the case of (anti-) protons the purity falls off as a function of p. Below $p < 2.5$ GeV/c the purity is around 100% . Above this value misidentifications happen, due to the merging of the TOF proton band with Kaons and later Pions. Here the purity is between 65% and 85%. For (anti-) deuteron the purity does not depend on p and stays flat at around 100%.
The efficiency is calculated by dividing the amount of identified particles by the amount of generated particles. In Figure 3.4 the efficiency of all four particle species as a function of p vs. η can be seen. Again, as a function of η, all efficiencies are flat and when looking at the momentum dependence, a kink can be seen when additionally requiring the TOF for PID. One can clearly see the different performances of identifying particles solely with the TPC and with TPC and TOF. A very significant amount of tracks are not matched to signals in the TOF. The main reason for this, is the large material budget of the Transition Radiation Detector (TRD), located between TPC and TOF. This trend can be seen for all particles except protons, where the efficiency stays flat around 25% over the whole momentum range. From previous analysis in all collision systems it is expected to follow a similar behavior close to that of antiprotons. Figure 3.6 shows the efficiency and purity corrected momentum distribution for all particle species. The correction is done by dividing the momentum spectra by the p dependent efficiencies and multiplying it by the p dependent purities. After this, it is expected to show an exponential behavior at the momentum region above 0.7 GeV/c. The kink that can be observed for protons and their antiparticles around $p \sim 1.0$ GeV/c is not expected. As

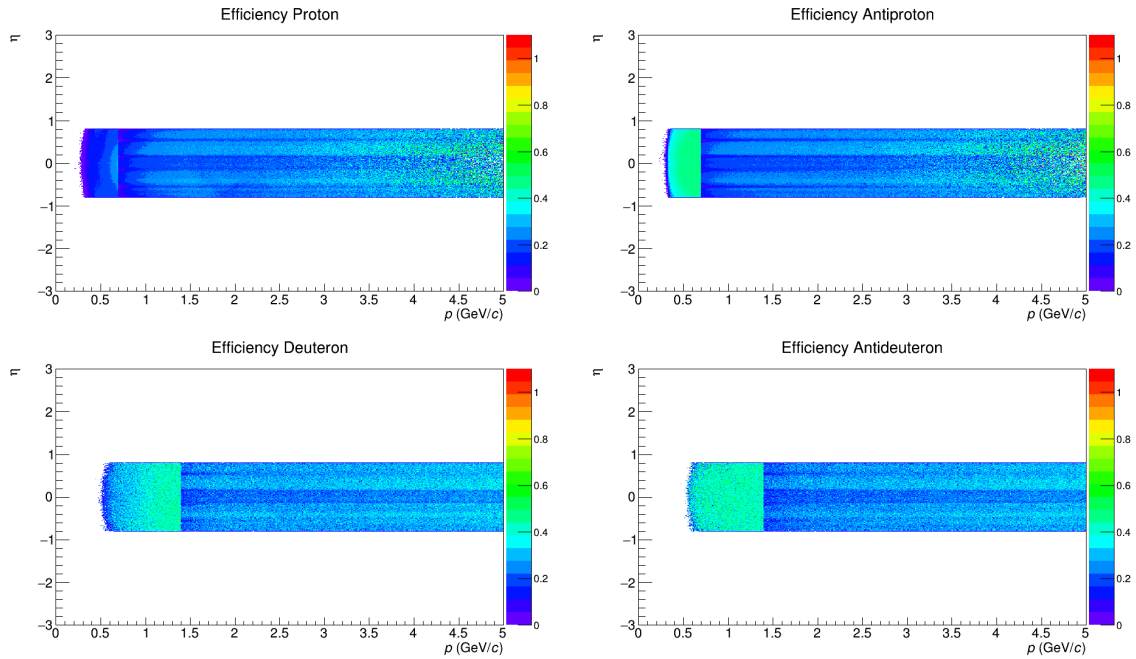

Figure 3.4.: Efficiency for all particles species in dependence of the momentum p and the pseudo rapidity η

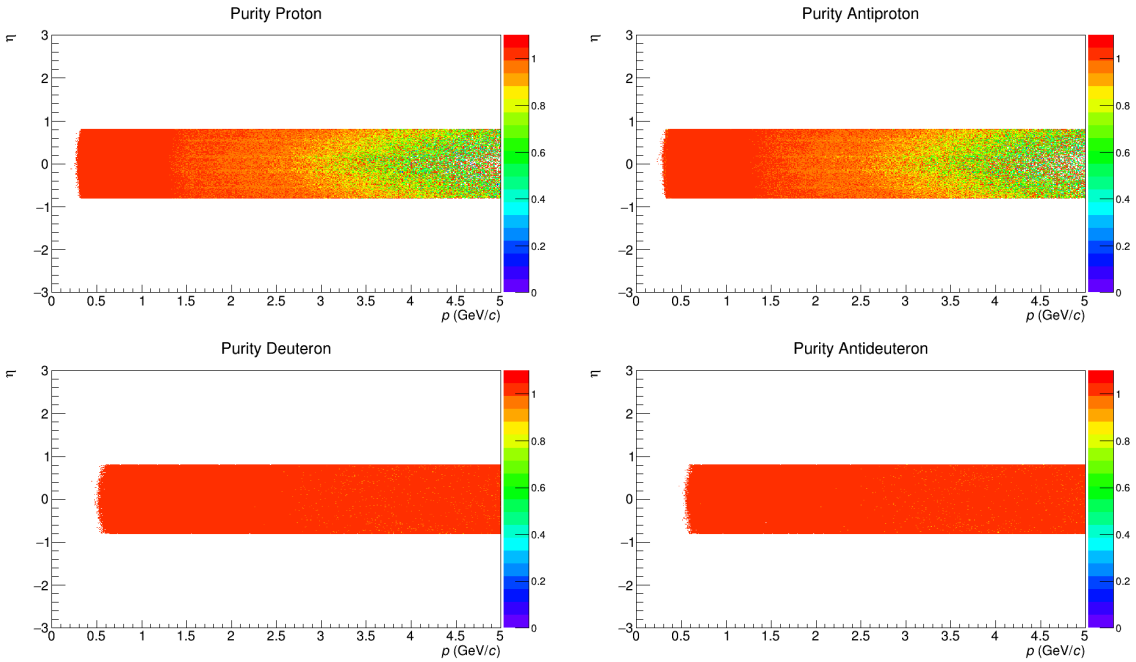

Figure 3.5.: Purity for all particles species in dependence of the momentum p and the pseudo rapidity η

it can be seen here, this is also not accounted for by the Monte Carlo simulation and therefore not corrected by purity of efficiency. This behavior was examined in more detail in the next section.

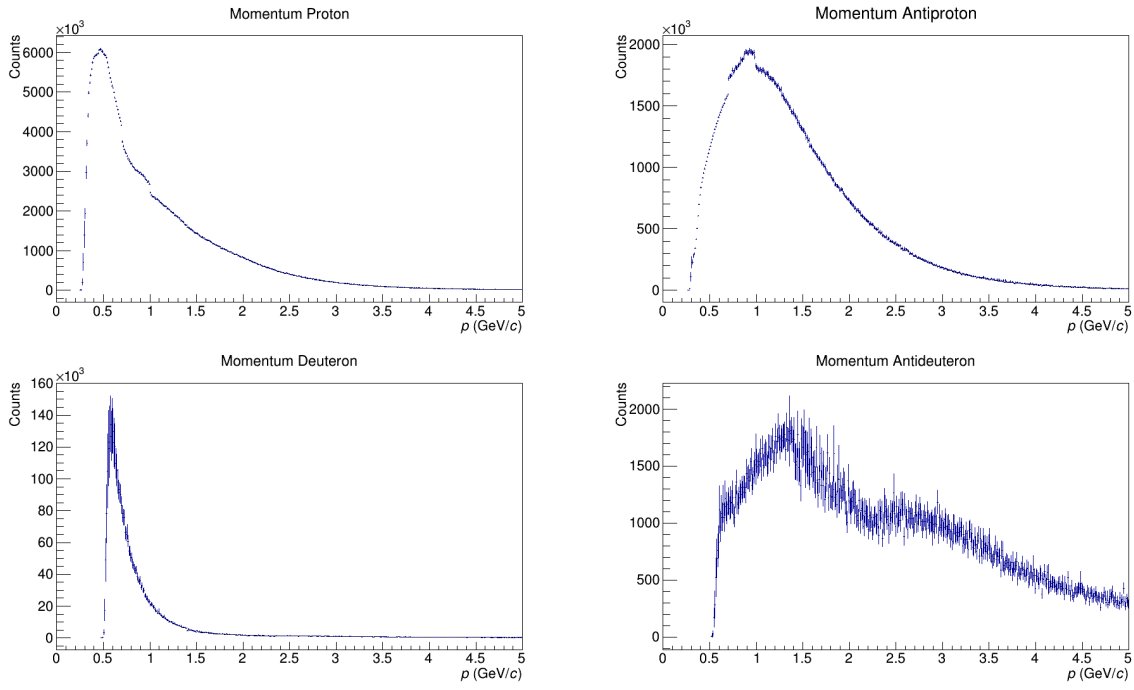

Figure 3.6.: Efficiency and purity corrected momenta spectra of all particle species

3.4. Momentum correction for the energy loss

As mentioned before the kink around $p \sim 1$ GeV/c in the momentum distribution of the (anti-) protons is unexpected and required some further investigation. Therefore the momentum at the inner wall of the TPC p_{inner} was compared to the momentum reconstructed at the collision vertex. In this section only (anti-) protons are considered. During the reconstruction of the tracks the momentum at the interaction vertex p and the momentum at the inner wall of the TPC p_{inner} is reconstructed. In Figure 3.7 the difference between these two momenta as a function of the vertex momentum p is shown. At the collision vertex the momentum p is always larger than at the inner wall of the TPC p_{inner}. While passing through the innermost detector system surrounding the interaction point the Inner Tracking System (ITS), a silicon tracker consisting of six layers, the particles loose energy and the momentum is reduced. This energy loss is described by the Bethe Bloch Formular and is used to propagate the momentum to the interaction vertex. When looking at the region around $p \sim 1.0$ GeV/c, where the kink in the momentum distribution was observed, the $p - p_{inner}$ distribution also shows irregularities.

When correcting the energy loss with the Bethe Bloch formula, a hypothesis on the particle mass is required. The assumed hypothesis for tracks during the reconstruction in the momentum region $p \sim 1$ GeV/c is shown in Figure 3.8. Most of the times for the selected (anti-) proton tracks the electron hypothesis was assumed for the correction. This is due to the fact, that only the TPC signal is used for PID during the reconstruction, and there the (anti-) proton and electron band merge in the momentum region $p \sim 1$ GeV/c. This leads to a wrong reconstructed momentum.

Therefore, a track-by-track correction for the energy loss is needed in this region. This correction is obtained by studying the energy loss discussed previously with Figure 3.7. Figure 3.9 shows the mean value of $p - p_{inner}$ as a function of the reconstructed track momentum. The line represents the empirical function

$$f(p) = A + B\left(1 + \frac{C}{p^2}\right)^D \tag{3.2}$$

used for the fit, from where the free parameters A, B, C and D were extracted. As mentioned before, this distribution follows the typical energy loss behavior $1/\beta^2 \propto 1/p^2$. The momentum is corrected on a track-by-track basis in the analysis by adding the mean deviation, for each p bin, from the corrected mean p value to the track momentum.

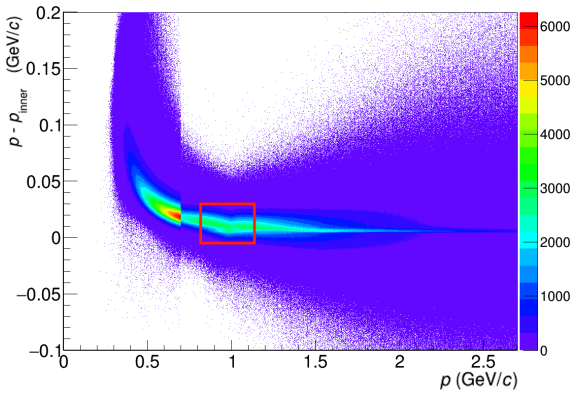

(a)

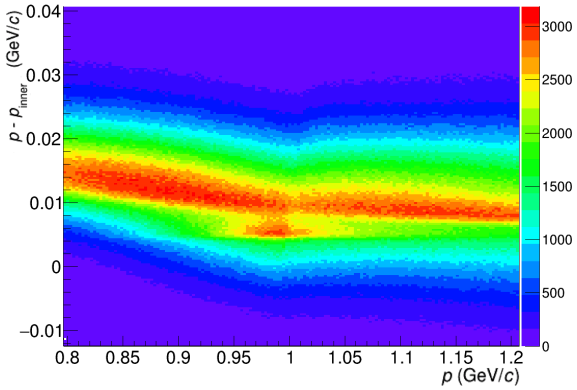

(b)

Figure 3.7.: (a)Difference of the reconstructed momentum and the momentum at the inner wall of the TPC, $p - p_{inner}$, as a function of the reconstructed momentum p The red rectangle focuses the region of interest. (b) Zoomed in region of interest with irregularities in the region $p - p_{inner} \approx 0.006$ GeV/c.

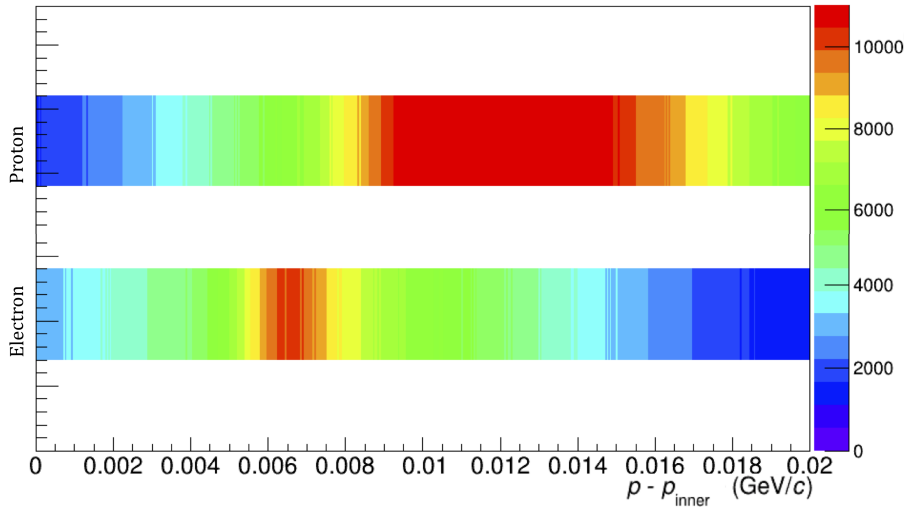

Figure 3.8.: The particle hypothesis obtained by PID with only the TPC as a function of $p - p_{inner}$ for the case of antiproton.

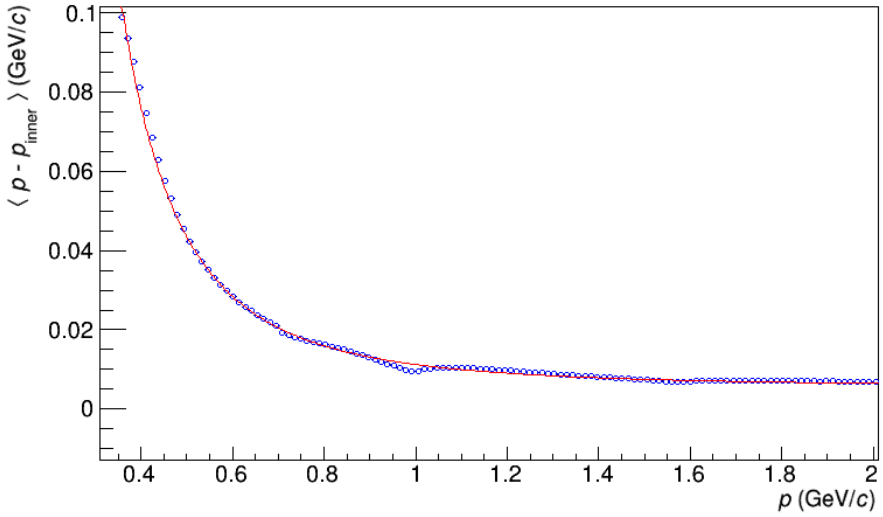

Figure 3.9.: The average difference between p and p_{inner} is plotted as a function of the reconstructed p for antiproton. The line represents a fit with the functional form as shown in Equation 3.2.

4. Results

In this chapter, the energy loss corrected momentum distribution is discussed. Then, an energy loss corrected efficiency and purity is reproduced. With this new efficiency and purity, the corrected momentum distribution is obtained.

4.1. Raw momentum distribution

After applying the track-by-track based momentum correction, the mean values of the reconstructed p as a function of $p - p_{inner}$, in the area of interest around $p \sim 1.0$ GeV/c, agree with the fit curve as can be seen in Figure 4.1.

The energy loss corrected raw momentum distribution of antiproton can be seen in Figure 4.2. The discontinuity, which is produced due to the additional requirement of matching the TPC track to the TOF signal remains the same, the discussed kink at $p \sim 1.0$ GeV/c however, is corrected. Since it worked for the raw momentum distribution, in a next step also the efficiency and purity were calculated again with the correction for the momentum propagation to obtain the corrected momentum distribution.

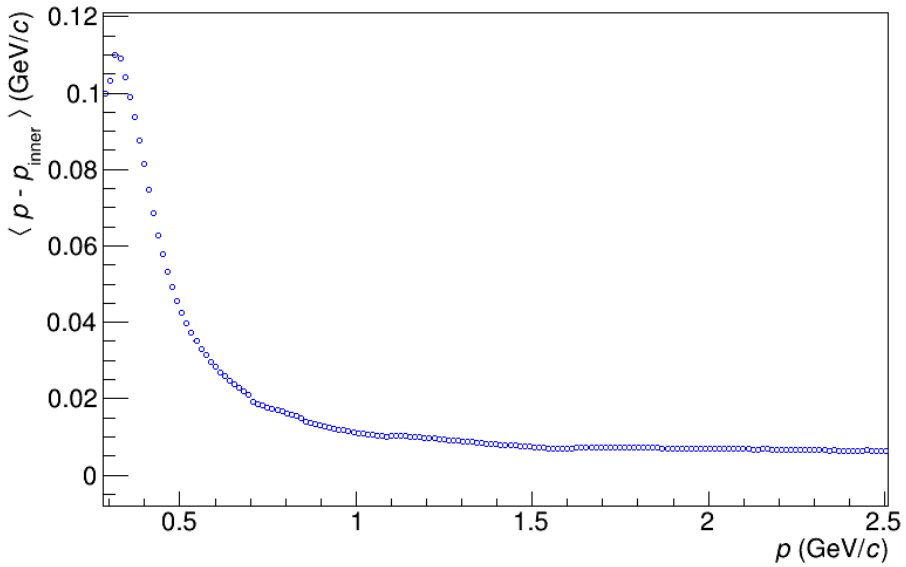

Figure 4.1.: The energy loss corrected average difference between p and p_{inner} is plotted as a function of the reconstructed p for antiproton corrected.

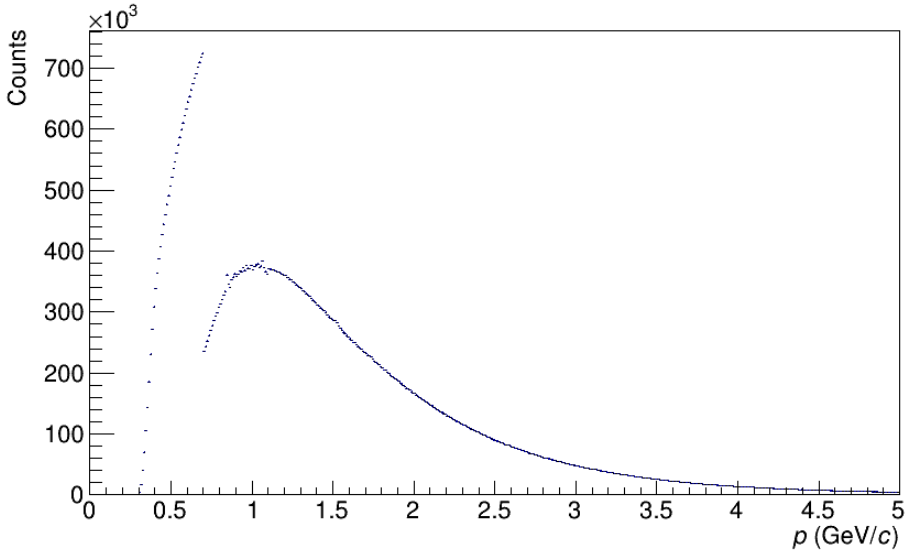

Figure 4.2.: Energy loss corrected raw momentum distribution of antiproton.

4.2. Corrected momentum distribution

In a last step the distribution obtained in Figure 4.2 has to be efficiency and purity corrected to get the momentum spectrum free of detector and acceptance effects. The efficiency and the purity are shown in Figure 4.3 and Figure 4.4 as a function of the momentum p. After the correction of the momentum propagated to the primary vertex, efficiency and purity, still follow the same behavior as discussed in section 3.3.

Since the masses are the same, the efficiencies of protons and antiprotons should follow a similar behavior. At low momenta, with TPC only PID , the efficiency is expected to be clearly higher than with the combined TPC and TOF PID. The efficiency of antiprotons follows this expected behavior. For protons however, it can be seen that the efficiency is about the same for the whole momentum region. After a thorough investigation of the track selection in the Monte Carlo data this could not be understood and therefore the antiproton efficiency was used to correct the proton momentum distribution.
Figure 4.5 shows the final spectra of all particle species with logarithmic scale in the y-axis. The (anti-) proton spectra follow an exponential distribution. Since the distributions are smooth at the momentum region $p \sim 1$ GeV/c, the energy loss correction still works after applying the efficiency and purity correction. The increased yield of protons when compared to antiprotons is expected due to additional contributions of material protons which are missing in the antiparticle spectra. To create an antiproton from material, an additional proton has to be created setting a much higher energy threshold compared to just scattering on a nucleus and creating a free proton.
Scattering data for (anti-) deuteron is very limited and is required as an input for the simulation in GEANT for the propagation of (anti-) deuteron through the detector and

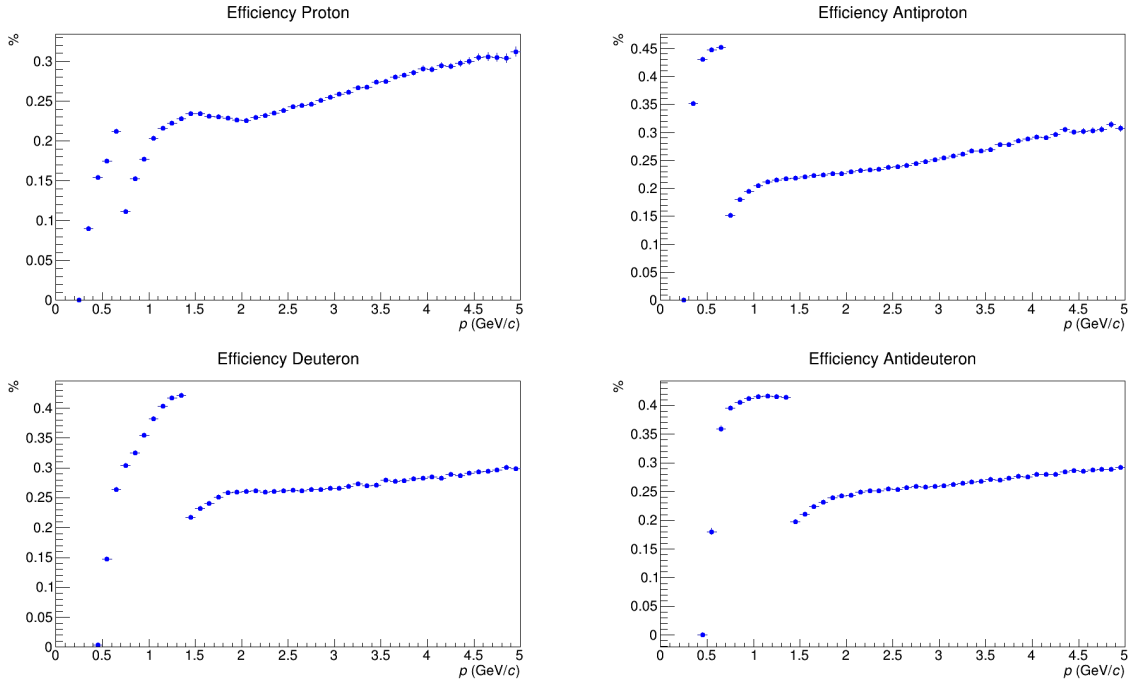

Figure 4.3.: Efficiency after the energy loss correction.

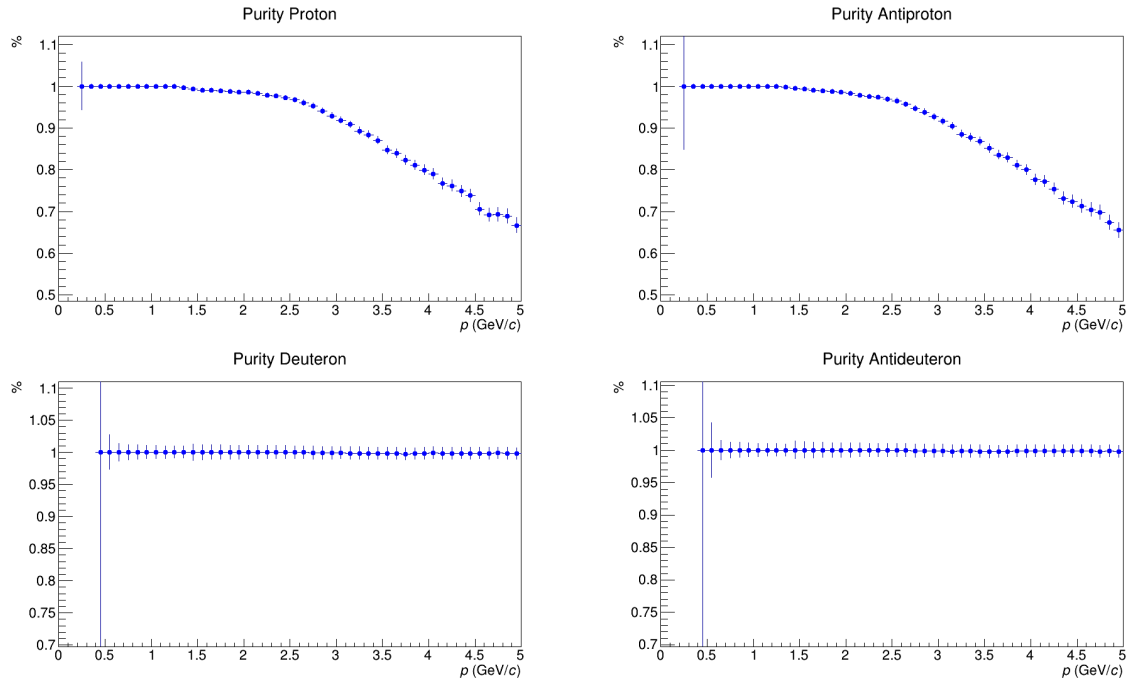

Figure 4.4.: Purity after the energy loss correction.

the resulting detector signals[15]. This might lead to the irregularities visible in the efficiency and purity corrected momentum spectra and needs further investigation.

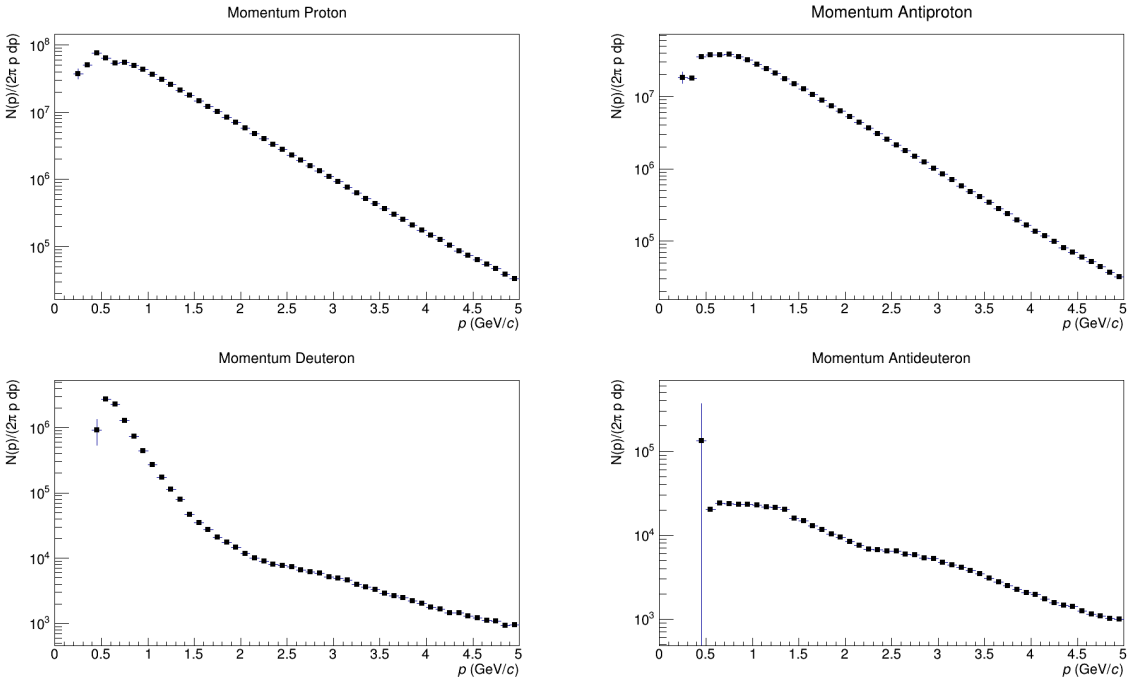

Figure 4.5.: Momenta spectra after the energy loss correction and the efficiency and purity correction.

5. Summary and Outlook

In summary, the spectral distributions of (anti-) protons and (anti-) deuterons in p-Pb collisions at $\sqrt{s_{NN}} = 5.02$ TeV have been presented. During the analysis a kink at the momentum region $p \sim 1.0$ GeV/c was found in the (anti-) proton spectrum. The source of it was unknown and therefore further investigated.
By looking at the mass hypothesis for the energy loss correction in the TPC, which is the only detector used for this, the source of this irregularities was found. In the region $p \sim 1.0$ GeV/c it was assumed an electron mass to correct protons and this led to a wrong energy loss correction. The correction was obtained with a fit to the data and implemented to correct the momentum track by track.
In a next step the track cuts implemented in this analysis need to be optimized in order to calculate the cross sections of protons, deuterons and the corresponding antiparticles. Specially the Monte Carlo data of (anti-) deuteron needs further investigation for a spectral distribution without irregularities. Finally, as presented in the introduction of this work, the analysis can focus on the conversions of antiparticles when interacting with the TRD material.

A. Analyzed Runs

The production cycle LHC16q_pass1_CENT_woSDD and the dataset with the following run numbers was used for the analysis:
265305, 265308, 265309, 265331, 265332, 265334, 265335, 265336, 265338, 265339, 265342, 265343, 265344, 265377, 265378, 265381, 265383, 265384, 265385, 265387, 265388, 265419, 265420, 265421, 265422, 265424, 265425, 265426, 265427, 265435, 265499, 265500, 265501, 265521, 265525.

The Monte Carlo production cycle LHC17f2b_fast was used to study the efficiency an purity of proton and antiproton. The following run numbers were used: 265309, 265332, 265334, 265335, 265336, 265338, 265339, 265342, 265343, 265344, 265377, 265378, 265381, 265383, 265384, 265385, 265387, 265388, 265419, 265420, 265421, 265422, 265424, 265425, 265426, 265427, 265435, 265499, 265500, 265501, 265521, 265525, 267163, 267164, 267165, 267166.

The Monte Carlo production cycle LHC17d10_fast was used to study the efficiency an purity of deuteron and antideuteron. The following run numbers were used:
265309, 265332, 265334, 265335, 265336, 265338, 265339, 265342, 265343, 265344, 265377, 265378, 265381, 265383, 265384, 265385, 265387, 265388, 265419, 265420, 265421, 265422, 265424, 265425, 265426, 265427, 265435, 265499, 265500, 265501, 265521, 265525, 267163, 267164, 267165, 267166.

Bibliography

[1] Vera C Rubin, Norbert Thonnard, et al. Motion of the galaxy and the local group determined from the velocity anisotropy of distant sc i galaxies. ii-the analysis for the motion. *The Astronomical Journal*, 81:719–737, 1976.

[2] Volker Springel, Simon D. M. White, et al. Simulating the joint evolution of quasars, galaxies and their large-scale distribution. Apr 2005.

[3] NASA/WMAP Science Team. Universe content - wmap 9yr pie chart, Aug 2013.

[4] T. Aramaki, S. Boggs, S. Bufalino, et al. Review of the theoretical and experimental status of dark matter identification with cosmic-ray antideuterons. 05 2015.

[5] C. Patrignani et al. (Particle Data Group). Plots of cross sections and related quantities. 2016.

[6] E. Gschwendtner, E. Adli, L. Amorim, et al. Awake, the advanced proton driven plasma wakefield acceleration experiment at cern. *Nuclear Instruments and Methods in Physics Research Section A: Accelerators, Spectrometers, Detectors and Associated Equipment*, 829(Supplement C):76 – 82, 2016. 2nd European Advanced Accelerator Concepts Workshop - EAAC 2015.

[7] J. Alme, Y. Andres, et al. The alice tpc, a large 3-dimensional tracking device with fast readout for ultra-high multiplicity events. *Nuclear Instruments and Methods in Physics Research Section A: Accelerators, Spectrometers, Detectors and Associated Equipment*, 622(1):316 – 367, 2010.

[8] J. Alme, Y. Andres, et al. The alice tpc, a large 3-dimensional tracking device with fast readout for ultra-high multiplicity events. page 55, 01 2010.

[9] ALICE Collaboration. Rapidity and transverse-momentum dependence of the inclusive j/ψ nuclear modification factor in p-pb collisions at $\sqrt{s_{NN}} = 5.02$ tev, 03 2015.

[10] ALICE Collaboration. Performance of the alice experiment at the cern lhc. 02 2014.

[11] R. Frühwirth. Application of kalman filtering to track and vertex fitting. *Nuclear Instruments and Methods in Physics Research Section A: Accelerators, Spectrometers, Detectors and Associated Equipment*, 262(2):444 – 450, 1987.

[12] Benjamin Andreas Hess, Hans Rudolf Schmidt, et al. Particle Identification in Jets and High-Multiplicity pp Events with the ALICE TPC, Jun 2015. Presented 09 Oct 2015.

[13] Stefan Roesler, Ralph Engel, and Johannes Ranft. The monte carlo event generator dpmjet-iii. page 6, December 2000.

[14] Rene Brun, L Urban, Federico Carminati, et al. Geant: Detector description and simulation tool. Technical report, CERN, 1993.

[15] ALICE Collaboration. Production of light nuclei and anti-nuclei in pp and pb-pb collisions at lhc energies. 06 2015.

List of Figures

List of Tables

Acknowledgements

At this point I would like to thank everyone who supported me during my thesis.
First of all, I would like to thank Prof. Laura Fabbietti, who enabled me to carry out this work and gave me the chance to take part in the FSP conference. This interesting and helpful experience gave me even more motivation to continue with the development of my work.
A special thanks goes to Bernhard Hohlweger who has supervised me throughout the thesis. He taught me how to program in C++ and answered all the questions I had. I thank him for all the time he has spent on my work over the last months.
I thank the whole working group for the great atmosphere.
Furthermore, I would like to thank all my friends, specially Mathias, Lukas, Felix and Linus for your patience and for all the conversations accompanied by a good coffee.
Thank you Aylin for the advices and the good energies you gave me.
Last but not least, I thank my family for the support during my physics study. Special thanks to my sister Lina for the moral support and to my parents for giving me the opportunity to study in Munich. Mamá, papá, muchas gracias por su apoyo incondicional.